DOI: http://dx.doi.org/10.1590/2179-10742017v16i3963

Time Reversal Imaging Based on the Space-Frequency ESPRIT

Tong Mu and Yaoliang Song
School of Electronic and Optical Engineering, Nanjing University of Science and Technology, Nanjing 210094, China. Tong Mu (mtonylucky@gmail.com); Yaoliang Song (ylsong@mail.njust.edu.cn)

***Abstract*—A novel time reversal approach for the point target imaging is proposed in this paper. This method requires only single measurement by the time reversal array, and it exploits the space-frequency decomposition plus the rotation invariance of the signal subspace for the target detecting. Numerical simulations are carried out to validate the imaging performance of the method for single target located at different positions in homogenous and continuous random medium respectively. The results indicate that the proposed method performs better than the conventional signal subspace based space-frequency algorithm both in imaging resolution and efficiency.**

***Index Terms*—**time reversal, space-frequency decomposition, ESPRIT algorithm, target imaging

I. INTRODUCTION

Time reversal (TR) techniques derive from acoustics [1] and they are introduced in the electromagnetic fields later [2]. They involve physical or synthetic retransmission of signals received by a TR antenna array in a time reversed fashion. These techniques exploit the invariance of the wave equation and enable the back-propagated signals to focus around the original source or target location. Due to the super resolution ability and self-adaptive focusing property [3], time reversal has a wide range of applications such as medical microwave imaging, long distance wireless communication, spatial power combining, etc.

The time reversal mirror (TRM) method back-propagates the TR signals directly and it detects the target by scanning the field value at each point in the probed domain [4]. The iterative TRM (ITRM) method conducts the signal reception, reversal and retransmission iteratively and makes the signals focus on the strongest target [5]. These methods implement time reversal in the time domain directly and result in an increase of the cost for signal processing and storage. Moreover, they are unable to detect weaker targets in multiple targets scenario.

The methods based on the TR operator obtained from the multistatic data matrix (MDM) is more effective for target imaging in complex environment. The singular value decomposition (SVD) of the TR operator lays the foundation of the decomposition of the TR operator (DORT) [6] and the TR multiple signal classification (TR-MUSIC) [7]. Eigenvectors of the signal subspace are utilized in the DORT to form the retransmitted signals and selective imaging for different targets can be achieved by

Brazilian Microwave and Optoelectronics Society-SBMO *received 10 Apr 2017; for review 13 Apr 2017; accepted 05 Aug 2017*
Brazilian Society of Electromagnetism-SBMag *ISSN 2179-1074*

DOI: http://dx.doi.org/10.1590/2179-10742017v16i3963

this method. The TR-MUSIC utilizes the noise subspace which is orthogonal to the signal subspace and it can detect multiple targets synchronously. However, to obtain the MDMs the probing signals need to be transmitted by each antenna in sequence and the target responses are recorded by all the antennas, making it time-consuming and difficult to detect the moving targets as well as active sources.

The methods based on the decomposition of the space-frequency MDM (SF-MDM) can overcome these defects [8], [9]. The SF-DORT conducts SVD to the SF-MDM obtained from single measurement to yield singular values and singular vectors. The left singular vectors span the signal subspace which encodes the target location in the form of the relative phase shifts among the antennas. The back-propagated signals for selective target imaging are constructed by using the left singular vectors and the frequency spectrum of the probing signal. The estimation of signal parameters via rotation invariance techniques (ESPRIT) exploits the rotation invariance of the signal subspace to estimate the orientation of targets [10]. It simplifies the procedure of pseudo-spectral searching and reduces the calculation costs [11].

In this paper, we propose a new space-frequency ESPRIT (SF-ESPRIT) method for point target imaging. The SF-MDM is obtained from only single measurement by TR array and then SVD is conducted to the matrix to yield the left singular vectors. Next, the TR array, the corresponding left singular vectors and the background Green functions are divided into two groups based on the subspace invariant principle of ESPRIT. At last, the rotation matrices are solved and the imaging function is given. The performance of the proposed method is examined by targets imaging simulations both in homogenous and continuous random media. Simulation results indicate that the SF-ESPRIT has higher imaging resolution than SF-DORT and it is also faster than SF-DORT thus it further improves the real-time capability for TR imaging.

II. TR IMAGING BASED ON THE SF-ESPRIT

We assume that there is a TR array consisting of N antennas, where N is even. And there are P targets in the probed domain, with $P<N$. The probing signal is transmitted by one antenna in the TR array, and all the antennas record the target response only once. Then the received signals are transformed into the frequency domain, forming the SF-MDM as follows:

$$\mathbf{K}=\begin{pmatrix} k_1(\omega_1) & k_1(\omega_2) & \cdots & k_1(\omega_M) \\ \vdots & \vdots & \ddots & \vdots \\ k_n(\omega_1) & k_n(\omega_2) & \cdots & k_n(\omega_M) \\ \vdots & \vdots & \ddots & \vdots \\ k_N(\omega_1) & k_N(\omega_2) & \cdots & k_N(\omega_M) \end{pmatrix} \tag{1}$$

The nth row of the matrix represents the sampling sequence in frequency domain of the signal received by the nth antenna, with $1\le n\le N$, and M is the number of sampling points. For each element $k(\omega)$ we have $\omega_1\le\omega\le\omega_M$, and the signal bandwidth is $\Omega=\omega_M-\omega_1$. Applying the SVD

Brazilian Microwave and Optoelectronics Society-SBMO *received 10 Apr 2017; for review 13 Apr 2017; accepted 05 Aug 2017*
Brazilian Society of Electromagnetism-SBMag *ISSN 2179-1074*

DOI: http://dx.doi.org/10.1590/2179-10742017v16i3963

to $\mathbf{K}$, we obtain that:

$$\mathbf{K} = \mathbf{U}\mathbf{\Lambda}\mathbf{V}^{\mathrm{H}} \tag{2}$$

where $\mathbf{\Lambda}$ is a $N \times M$ real diagonal matrix, and the elements on the main diagonal of $\mathbf{\Lambda}$ are singular values. $\mathbf{U}$ is a $N \times N$ matrix, and each column of $\mathbf{U}$ is a left singular vector, forming an orthonormal set which spans the antenna location space. $\mathbf{V}$ is a $M \times M$ matrix, and each column of $\mathbf{V}$ is a right singular vector, forming an orthonormal set which spans the signal frequency space. Here $\mathbf{U}$ represents the spatial relationship between the TR array and the targets.

In fact, $\mathbf{K}$ can be seen as a mapping from the signal frequency space to the antenna space:

$$\mathbf{K}\mathbf{V}_p = \lambda_p \mathbf{U}_p \tag{3}$$

where $\mathbf{V}_p$ is a $M \times 1$ right singular vector, λ_p is the pth singular value, and $\mathbf{U}_p$ is a $N \times 1$ left singular vector with $p = 1, ..., P$, corresponding to P non-zero singular values. Therefore, $\mathbf{U}_p$ spans the signal subspace, and $\mathbf{U}_{p'}$ with $p' = P+1, ..., N$ spans the noise subspace. For certain $\mathbf{U}_p$, the N elements contain the relative phase shift information among the antennas in TR array. If the probing signal is defined as $s(t)$ and the frequency spectrum is $S(\omega)$, the TR signal retransmitted by the TR array can be obtained by multiplying $S(\omega)$ by $\mathbf{U}_p$, which is equivalent to conducting the amplitude and phase weighting to the probing signal:

$$\mathbf{r}_{TR}(\omega) = \mathbf{U}_p S(\omega) \tag{4}$$

Back propagating $\mathbf{r}_{TR}(\omega)$ to the probed domain, selective imaging for different targets can be achieved by choosing different $\mathbf{U}_p$ to construct the back-propagated signal.

For target imaging, the prior knowledge of the background Green's function at each searching point $\mathbf{X}_s$ in the probed domain is required. We define $G(\mathbf{X}_s, \mathbf{X}_n, \omega)$ as the background Green's function, where $\mathbf{X}_n$ is the location of the nth antenna. Considering all the antennas, we have:

$$\mathbf{g}(\mathbf{X}_s, \omega) = [G(\mathbf{X}_s, \mathbf{X}_1, \omega), ..., G(\mathbf{X}_s, \mathbf{X}_N, \omega)]^{\mathrm{T}} \tag{5}$$

$\mathbf{g}(\mathbf{X}_s, \omega)$ contains the spatial information of each searching point, and it is dependent on the angular frequency ω. The imaging pseudo-spectral of SF-DORT is defined as:

$$\mathbf{D}_{SF-DORT}(\mathbf{X}_s) = \int_{\Omega} \left\langle \mathbf{g}(\mathbf{X}_s, \omega), \mathbf{r}_{TR}(\omega) \right\rangle d\omega \tag{6}$$

where $\langle \cdot \rangle$ denotes the inner product.

The ESPRIT exploits the rotation invariance of the signal subspace which is derived from the translation invariance of the antenna array. Particularly, an array is divided into two subarrays which contain identical number of antennas. Each corresponding element in the two subarrays has same spatial displacement, which means that the rotation matrix is the only difference between the two subarrays. In our model, we divide the TR array containing N antennas into two subarrays which

DOI: http://dx.doi.org/10.1590/2179-10742017v16i3963

both comprise $\frac{N}{2}$ antennas. Then the left singular vector corresponding to the pth target is divided as follows:

$$\mathbf{U}_p = \begin{bmatrix} \mathbf{U}_{p1} \\ \mathbf{U}_{p2} \end{bmatrix} \tag{7}$$

where $\mathbf{U}_{p1}$ and $\mathbf{U}_{p2}$ are $\frac{N}{2}\times 1$ vectors. Similarly, the background Green's function is divided as follows:

$$\mathbf{g}(\mathbf{X}_s, \omega) = \begin{bmatrix} \mathbf{g}_1(\mathbf{X}_s, \omega) \\ \mathbf{g}_2(\mathbf{X}_s, \omega) \end{bmatrix} \tag{8}$$

where $\mathbf{g}_1(\mathbf{X}_s, \omega)$ and $\mathbf{g}_2(\mathbf{X}_s, \omega)$ are also $\frac{N}{2}\times 1$ vectors. Then two $\frac{N}{2}\times\frac{N}{2}$ diagonal matrices $\mathbf{\Phi}_U$ and $\mathbf{\Phi}_g$ are introduced and satisfy that:

$$\mathbf{U}_{p1} = \mathbf{\Phi}_U \cdot \mathbf{U}_{p2} \tag{9}$$

$$\mathbf{g}_1(\mathbf{X}_s, \omega) = \mathbf{\Phi}_g \cdot \mathbf{g}_2(\mathbf{X}_s, \omega) \tag{10}$$

Therefore, if we let φ_i and ϕ_i be the ith element on the main diagonal of $\mathbf{\Phi}_U$ and $\mathbf{\Phi}_g$ respectively, the imaging pseudo-spectral of SF-ESPRIT is formed by calculating the relative error between φ_i and ϕ_i at each searching point in the probed domain:

$$\mathbf{D}_{SF-ESPRIT}(\mathbf{X}_s) = \left(\sum_{i=1}^{N/2} \left| \frac{|\phi_i(\mathbf{X}_s)| - |\varphi_i|}{|\varphi_i|} \right| \right)^{-1} \tag{11}$$

When the searching point happens to be the target position, the relative error in Equation (11) tends to zero, and the pseudo-spectral reaches the peak. If the pseudo-spectral is calculated for all searching points, the imaging for the pth target is achieved. The imaging performance depends on the contrast between the relative error calculated at the target position and non-target positons. For realizing high resolution, we revise the background Green's function by

$$G(\mathbf{X}_p, \mathbf{X}_n, \omega) = \frac{e^{j\gamma|\mathbf{X}_p - \mathbf{X}_n|}}{|\mathbf{U}_p^n| 4\pi |\mathbf{X}_p - \mathbf{X}_n|} \tag{12}$$

where γ is the wave number, and $|\mathbf{U}_p^n|$ is the amplitude of the nth element of $\mathbf{U}_p$. $\mathbf{X}_p$ and $\mathbf{X}_n$ are the positions of the pth target and the nth antenna respectively.

III. RESULTS AND DISCUSSIONS

Figure 1 shows the model used in the imaging experiments. We consider single target imaging in both homogenous and random medium. We use the finite difference time domain (FDTD) method to calculate the electromagnetic scattering and obtain the target response. The probed domain is 2m ×

  ISSN 2179-1074

DOI: http://dx.doi.org/10.1590/2179-10742017v16i3963

2m and the point target with relative permittivity of $\varepsilon_r = 8.3$ is embedded in the media. The relative permittivity of the homogenous media is set as ε_m=2.9. The random media is modeled by spatially fluctuating permittivity $\varepsilon(\vec{r}) = \varepsilon_m + \varepsilon_f(\vec{r})$, where $\vec{r} = x\hat{x} + y\hat{y}$ is the spatial position [12]. The fluctuating term $\varepsilon_f(\vec{r})$ is the zero-mean Gaussian random variable with Gaussian correlation function given by:

$$C(\vec{r}_1 - \vec{r}_2) = \left\langle \varepsilon_f(\vec{r}_1)\varepsilon_f^*(\vec{r}_2) \right\rangle = \delta \exp(-(|x_1 - x_2|^2 + |y_1 - y_2|^2)/l_s^2) \tag{13}$$

where δ is the variance and l_s is the correlation length. The probing signal is a modulated Gaussian pulse with center frequency of 600MHz, and the number of sampling points is set as 2000. The linear TR array contains six antennas located at (0.05m, 0.5m), (0.05m, 0.64m), … , (0.05m, 1.2m) respectively. They are separated by 0.14m which is half of the wave length corresponding to the center frequency of the probing signal in homogenous media. The FDTD grid size is set as $\Delta x = \Delta y = 1\text{cm}$, and the perfectly matched layer (PML) is applied as the boundary condition to avoid the wave reflection on the boundary of the probed domain.

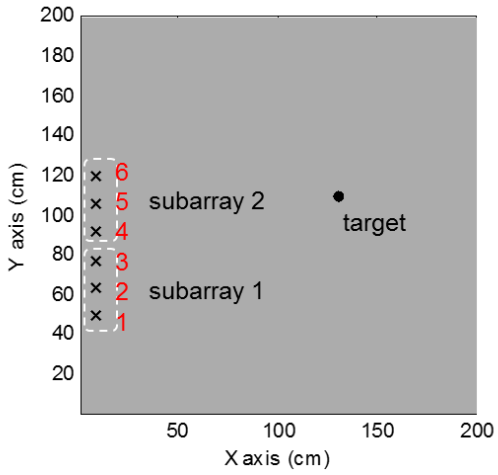

Fig. 1. Illustration of the TR array and the target.

The simulation is carried out for the target located at (0.53m, 1.26m) and (0.91m, 0.39m) in homogenous and random media respectively. The pulse is transmitted by the 3th antenna and the scattered signals are recorded by all the antennas only once. The received signals are used to construct the SF-MDM according to Equation (1). Applying SVD to the SF-MDM, we obtain the singular values and the left singular vector $\mathbf{U}_1$. Next we divide the TR array into two subarrays. The first subarray contains the 1st, 2nd and 3rd antenna, and the second one contains the 4th, 5th and 6th antenna. Then the background Green's function and $\mathbf{U}_1$ are divided into two groups corresponding to the two subarrays. At last the rotation matrices are solved and they are utilized to calculate the pseudo-spectrum according to Equation (11). The imaging results of the SF-ESPRIT in homogenous media are shown in Fig. 2, and they are compared with the conventional SF-DORT method. All the

DOI: http://dx.doi.org/10.1590/2179-10742017v16i3963

pseudo-spectrums are normalized to 1, and the actual position of the target is marked with "○" in each figure.

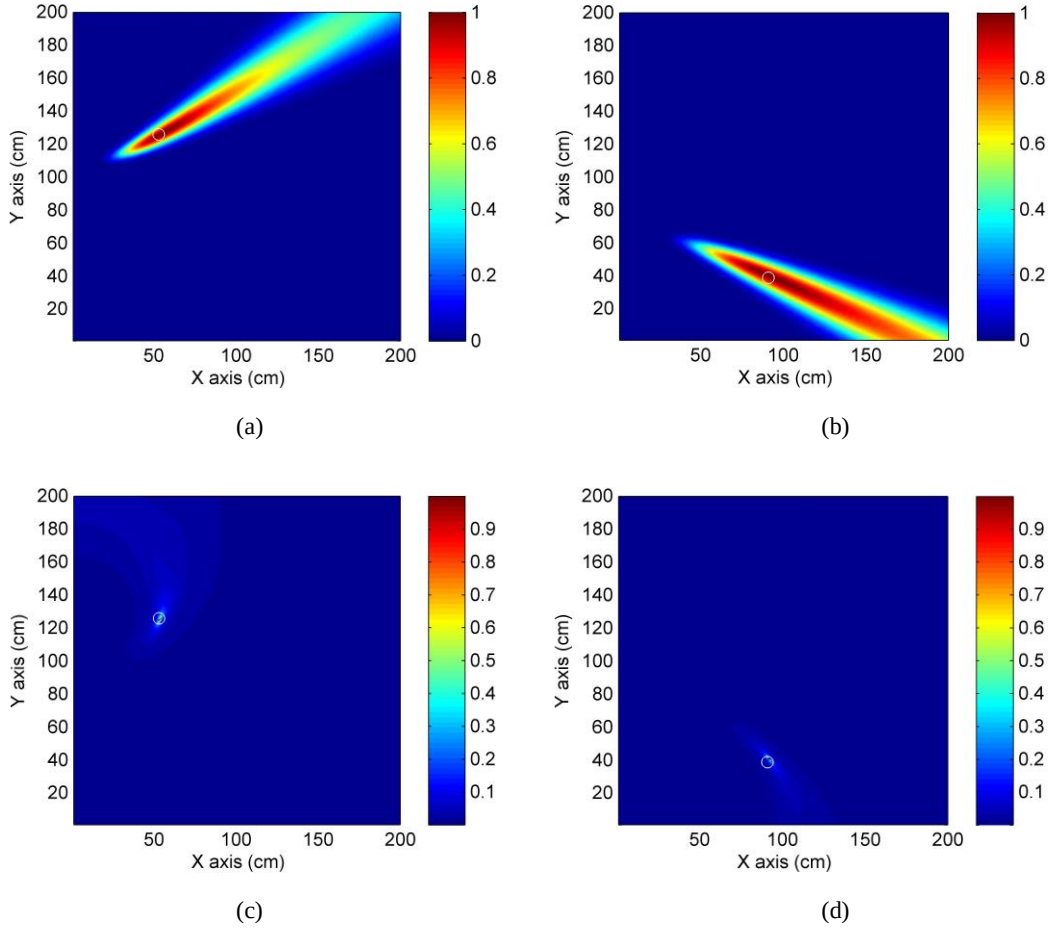

Fig. 2. The imaging results in homogeneous media. (a) The SF-DORT image of the target located at (0.53m, 1.26m); (b) The SF-DORT image of the target located at (0.91m, 0.39m); (c) The SF-ESPRIT image of the target located at (0.53m, 1.26m); (d) The SF-ESPRIT image of the target located at (0.91m, 0.39m).

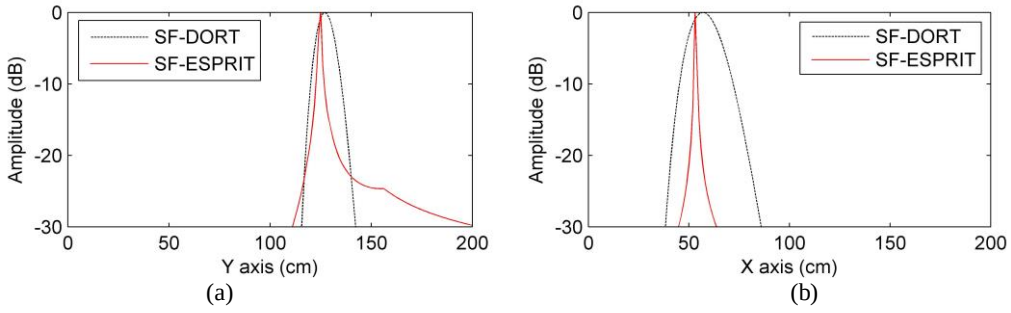

Fig. 3. Resolution comparisons between SF-DORT and SF-ESPRIT for the target located at (0.53m, 1.26m). (a) Lateral resolution; (b) Longitudinal resolution.

DOI: http://dx.doi.org/10.1590/2179-10742017v16i3963

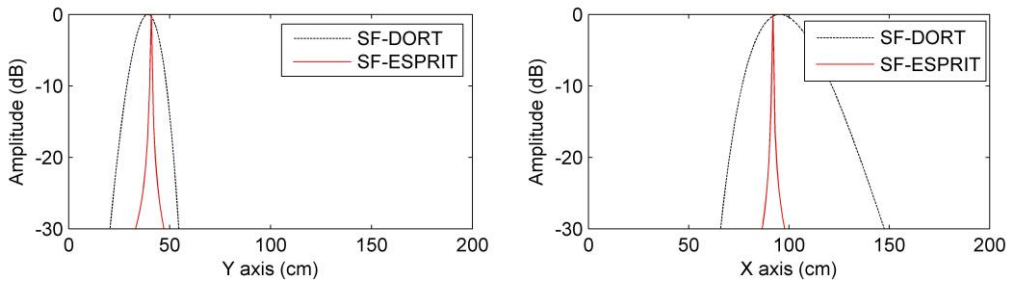

Fig. 4. Resolution comparisons between SF-DORT and SF-ESPRIT for the target located at (0.91m, 0.39m). (a) Lateral resolution; (b) Longitudinal resolution.

From Fig. 2 we can see that both SF-DORT and SF-ESPRIT can give accurate location of the target. However, the SF-DORT image has blade shape and long trailing which are not observed in the SF-ESPRIT image. Lateral and longitudinal resolution of the two methods are given in Fig. 3 and Fig. 4 for different target positions (normalized to dB). It can be observed that SF-ESPRIT has much higher resolution than SF-DORT in both lateral and longitudinal.

If the TR array is divided as follows: the first subarray contains the 1st, 2nd and 3rd antenna and the second one contains the 6th, 5th and 4th antenna, rotation matrices which are different from Equation (9) and (10) can be obtained. Then the new rotation invariance is exploited to calculate the pseudo-spectral. We revise the imaging function by multiplying the new pseudo-spectral by the old one, and the imaging results of the revised SF-ESPRIT are shown in Fig. 5. It can be seen from Fig. 5 (a) and (b) that the revised SF-ESPRIT has narrower and sharper pseudo-spectral at the target position, which provides better focusing performance. Figure 5 (c) and (d) show the imaging results of the target located at (0.53m, 1.26m) and (0.91m, 0.39m) respectively based on the revised SF-ESPRIT, and the partial figure is zoomed in to show the focusing details clearly.

In addition, the Monte-Carlo simulations are carried out for 1000 times on the PC with CPU frequency of 3.3GHz and RAM of 6GHz. It turned out that the SF-DORT takes 2995ms in average, while the SF-ESPRIT takes 1143ms in average. Therefore the SF-ESPRIT has higher detecting efficiency and it further improves the real-time capability for TR imaging.

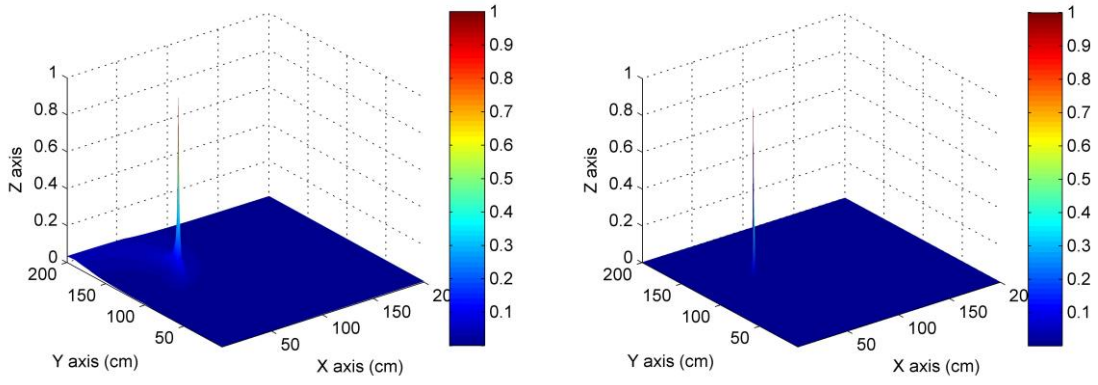

received 10 Apr 2017; for review 13 Apr 2017; accepted 05 Aug 2017

ISSN 2179-1074

DOI: http://dx.doi.org/10.1590/2179-10742017v16i3963

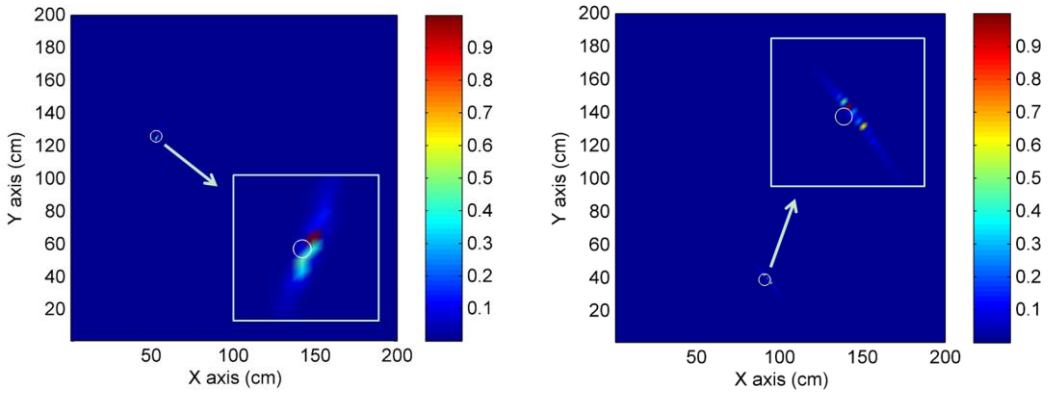

(c) (d)

Fig. 5. (a) Three-dimensional pseudo-spectrum given by the SF-ESPRIT; (b) Three-dimensional pseudo-spectrum given by the revised SF-ESPRIT; (c) The revised SF-ESPRIT image of the target located at (0.53m, 1.26m); (d) The revised SF-ESPRIT image of the target located at (0.91m, 0.39m).

Then we consider the scenario of the random media where the fluctuating parameters are set as δ=0.03 and $l_s = 8\Delta x$. The distribution of singular values gained in homogeneous and random media are shown in Fig. 6 (a). It can be seen that there is only one large (non-zero) singular value in both the mediums as there is a single target. The target responses recorded by the 5th antenna are shown in Fig. 6 (b). It can be seen that there are more ripples in the response recorded in random media than homogeneous media. Figure 7 shows the imaging results of SF-DORT and SF-ESPRIT in random media. Similarly, both the two methods can locate the target precisely in random media. The SF-DORT shows stronger robustness as the resolution is almost as same as that in homogenous media. The resolution of SF-ESPRIT declines to some degree in random medium. It is because that the multiple scattering caused by the random medium deviates the phase of each element of $\mathbf{U}_1$ which contains the information of the relationship between the target and the TR array. Thus, the rotational invariance is weakened and the imaging resolution drops off.

For evaluating the performance of the SF-ESPRIT in random media comprehensively, we change the fluctuating parameters and the results are shown in Fig. 8. Figure 8 (a) and (b) show the images of the target with δ=0.06 and $l_s = 8\Delta x$, and Fig. 8 (c) and (d) show the images of the target with δ=0.03 and $l_s = 20\Delta x$. The results indicate that larger variance or correlation length may cause lower imaging resolution, but the target can still be located accurately by SF-ESPRIT. Furthermore, the SF-ESPRIT provides higher resolution than SF-DORT even in stronger fluctuating environment.

  ISSN 2179-1074

DOI: http://dx.doi.org/10.1590/2179-10742017v16i3963

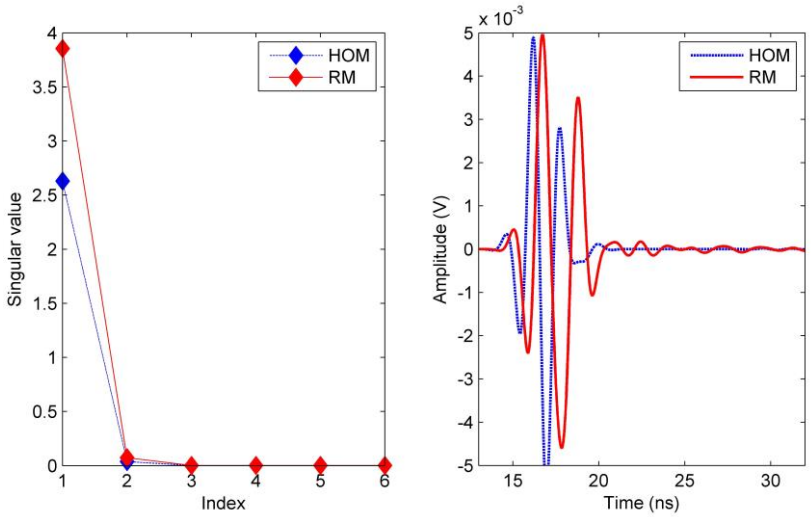

(a) (b)

Fig. 6. (a) The distribution of singular values; (b) Target responses received by the 5th antenna.

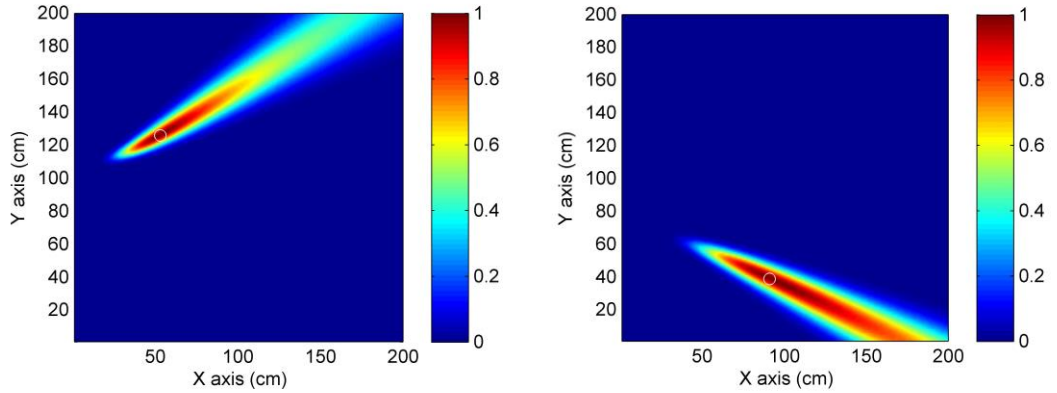

(a) (b)

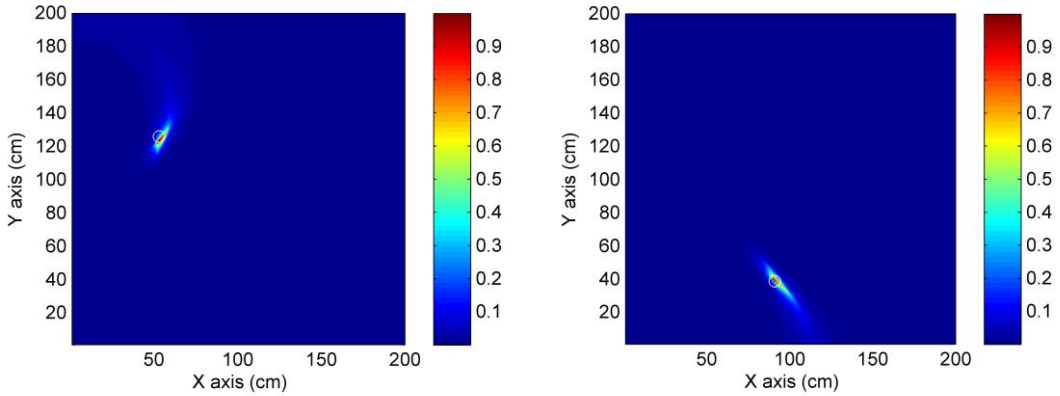

(c) (d)

Fig. 7. The imaging results in random media. (a) The SF-DORT image of the target located at (0.53m, 1.26m); (b) The SF-DORT image of the target located at (0.91m, 0.39m); (c) The SF-ESPRIT image of the target located at (0.53m, 1.26m); (d) The SF-ESPRIT image of the target located at (0.91m, 0.39m).

DOI: http://dx.doi.org/10.1590/2179-10742017v16i3963

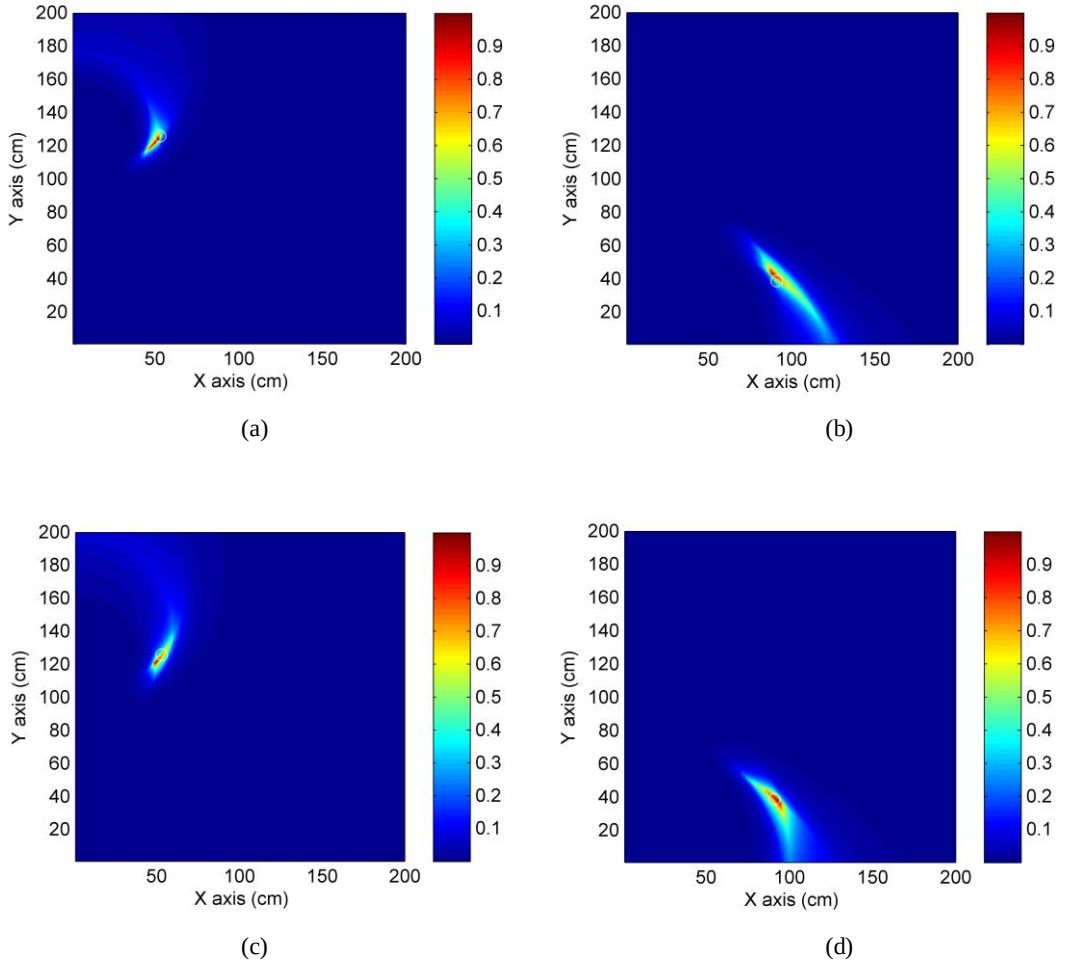

Fig. 8. The SF-ESPRIT imaging results in different random media. (a) The image of the target located at (0.53m, 1.26m) with δ=0.06 and $l_s = 8\Delta x$; (b) The image of the target located at (0.91m, 0.39m) with δ=0.06 and $l_s = 8\Delta x$; (c) The image of the target located at (0.53m, 1.26m) with δ=0.03 and $l_s = 20\Delta x$; (d) The image of the target located at (0.91m, 0.39m) with δ=0.03 and $l_s = 20\Delta x$.

IV. CONCLUSIONS

A new TR imaging method based on the SF-ESPRIT is proposed in this paper. The method requires only single measurement by the TR array for the SF-MDM acquisition and the imaging function is constructed based on the rotation invariance of the signal subspace. By using a linear TR array containing only six antennas, we achieve high resolution imaging for the point target located at different positions. The imaging resolution in homogenous media can be further promoted by using the revised imaging function. The comparisons of the imaging results between SF-ESPRIT and SF-DORT indicate that the SF-ESPRIT has better imaging performance in both homogenous and random media and also has faster speed than the conventional SF-DORT. Therefore, the SF-ESPRIT has an application potential for microwave tumor detection, buried target localization, moving target tracking, etc. Further researches include extending the method to multiple targets detection and experimental verification.

DOI: http://dx.doi.org/10.1590/2179-10742017v16i3963

ACKNOWLEDGMENT

This work was supported by the National Natural Science Foundation of China under Grant 61271331 and Grant 61571229.

REFERENCES

[1] Fink M, Cassereau D, Derode A, et al. Time-reversed acoustics[J]. Reports on progress in Physics, 2000, 63(12): 1933.
[2] Lerosey G, De Rosny J, Tourin A, et al. Time reversal of electromagnetic waves[J]. Physical review letters, 2004, 92(19): 193904.
[3] Lerosey G, De Rosny J, Tourin A, et al. Focusing beyond the diffraction limit with far-field time reversal[J]. Science, 2007, 315(5815): 1120-1122.
[4] Kosmas P, Rappaport C M. Time reversal with the FDTD method for microwave breast cancer detection[J]. IEEE Transactions on Microwave Theory and Techniques, 2005, 53(7): 2317-2323.
[5] Zhu X, Zhao Z, Yang W, et al. Iterative time-reversal mirror method for imaging the buried object beneath rough ground surface[J]. Progress In Electromagnetics Research, 2011, 117: 19-33.
[6] Yavuz M E, Teixeira F L. Full time-domain DORT for ultrawideband electromagnetic fields in dispersive, random inhomogeneous media[J]. IEEE Transactions on Antennas and Propagation, 2006, 54(8): 2305-2315.
[7] Ciuonzo D, Romano G, Solimene R. Performance analysis of time-reversal MUSIC[J]. IEEE Transactions on Signal Processing, 2015, 63(10): 2650-2662.
[8] Yavuz M E, Teixeira F L. Space–frequency ultrawideband time-reversal imaging[J]. IEEE Transactions on Geoscience and Remote Sensing, 2008, 46(4): 1115-1124.
[9] Zhong X, Liao C, Lin W. Space-Frequency Decomposition and Time-Reversal Imaging[J]. IEEE Transactions on Antennas and Propagation, 2015, 63(12): 5619-5628.
[10] Roy R, Kailath T. ESPRIT-estimation of signal parameters via rotational invariance techniques[J]. IEEE Transactions on acoustics, speech, and signal processing, 1989, 37(7): 984-995.
[11] Gao W, Wang X H, Wang B Z. Time-reversal ESPRIT imaging method for the detection of single target[J]. Journal of Electromagnetic Waves and Applications, 2014, 28(5): 634-640.
[12] Moss C D, Teixeira F L, Yang Y E, et al. Finite-difference time-domain simulation of scattering from objects in continuous random media[J]. IEEE Transactions on Geoscience and Remote Sensing, 2002, 40(1): 178-186.

